INTERNATIONAL JOURNAL FOR NUMERICAL METHODS IN FLUIDS
Int. J. Numer. Meth. Fluids 2005; **47**:1181–1187
Published online 1 February 2005 in Wiley InterScience (www.interscience.wiley.com). DOI: 10.1002/fld.901

A high-order TVD transport method for hybrid meshes on complex geological geometry

S. K. Matthäi, A. A. Mezentsev*,†, C. C. Pain and M. D. Eaton

Department of Earth Sciences and Engineering, Imperial College London, Exhibition Road, SW7 2AZ London, U.K.

SUMMARY

The paper presents a new implicit pressure–implicit saturation higher-order accurate in space and second-order accurate in time advection–dispersion scheme for the hyperbolic transport equations in porous media with discrete three-dimensional representation of material interfaces. We develop adaptive time differencing methods to use time steps greater than the mesh Courant number (Courant–Friedrich–Levy condition, CFL). The paper pays special attention to hybrid discretization of subsurface geometry, placing emphasis on the multiphase flow in fractured petroleum reservoirs. We also introduce numerical iso-parametric double mapping integration method for node-centred hybrid meshes and use it in our transport scheme. Copyright © 2005 John Wiley & Sons, Ltd.

KEY WORDS: control volume finite element method; hybrid mesh; second-order time discretization

1. INTRODUCTION

Much of the world's remaining oil reserves are hosted by fractured reservoirs, such as the Persian Gulf reservoirs [1]. Extraction of oil from such reservoirs can terminate abruptly when injected water invades the fractures, trapping the oil inside. Laboratory experiments on fractured rocks are difficult and expensive to conduct and numerical models have become the preferred tool for the investigation of transport phenomena in complex reservoirs [2–4].

Structured grids simply do not have the ability to capture curved features of fracture geometry. Applications of the unstructured transport schemes in the subsurface include the control volume method (CVM) [2], the control volume finite element method (CVFEM) [3], the finite element method (FEM) [4], but most of the models are still restricted to 2D. The problem of 3D modelling of subsurface flow is two-fold: firstly, usage of an automatic 3D unstructured

*Correspondence to: Andrey A. Mezentsev, Department of Earth Sciences and Engineering, Imperial College London, Exhibition Road, SW7 2AZ London, U.K.
†E-mail: a.mezentsev@imperial.ac.uk

Contract/grant sponsor: Industrial Technology Facilitator, ITF

Received 27 April 2004
Revised 24 November 2004
Accepted 30 November 2004

mesh generation is not yet established in the area, secondly, it requires robust high-order non-oscillatory transport schemes with time steps larger than Courant number (CN) of the grid. The present paper develops such methods.

2. METHODS

2.1. Governing equations

Nomenclature of symbols in equations is given in Table I.

Like Reference [4] we compute transient fluid pressure diffusion and immiscible displacement of slightly compressible phases in a sequential manner. Firstly, an elliptic–parabolic pressure equation is solved to obtain a total velocity of fluid phases, $\mathbf{v}_t$, via Darcy's law, taking into account buoyancy contributions due to fluid density, ρ:

$$\mathbf{v}_t = -\lambda_t[\nabla p + \mathbf{g}\rho] = -\lambda_t \nabla p_r \tag{1}$$

Reduced pressure is defined as $p_r = p - \rho_0 \mathbf{g}$. The gradient of p_r is derived from p_r-saturation relationships, varying among rock types. The conservation of total fluid volume in slightly compressible flow requires

$$\nabla \cdot \mathbf{v}_t - \dot{\mathbf{q}} = 0 \tag{2}$$

By substituting Darcy's law for $\mathbf{v}_t$ we obtain

$$-\nabla \cdot \lambda_t \nabla p - \dot{\mathbf{q}} = 0 \tag{3}$$

The total mobility, λ_t, requires a knowledge of the permeability tensor $\mathbf{K}$, relative permeability multipliers for each phase, k_{ri}, and their viscosities μ_i, for non-wetting and wetting phases. The calculation of k_{ri} relies on experimentally parameterized models like those in Reference [5], and others, relating capillary pressure of phases to saturation. For transient pressure diffusion Equation (3) becomes

$$\phi c_t \frac{\partial p_r}{\partial t} = -\nabla \cdot (\mathbf{K}\lambda_t \nabla p_r) + \dot{\mathbf{q}} \tag{4}$$

Table I. Nomenclature of symbols, used in equations.

Symbol	Meaning	Symbol	Meaning
$\mathbf{v}_t$	Total velocity	p	Fluid pressure
λ_t	Total mobility of fluid	$\mathbf{g}$	Gravity acceleration
$\mathbf{K}$	Permeability tensor	ρ_r	Average fluid density
k_{ri}	Permeability multiplier	μ_i	Viscosity of phase $i = n, w$
$\mathbf{f}_i$	Fractional flow for phase $i = n, w$	ϕ	Porosity of the rock
$\dot{\mathbf{q}}$	Volume source term	ψ_i	Saturation phase $i = n, w$
M_i	Interpolation function for CV i	$\mathbf{n}$	Normal to the CV facet
$\mathbf{M}$	Vector of CV interpolation functions	Θ	Time stepping parameter

where c_t is the total system compressibility above the bubble point. The subscripts r in the pressure equation (4), denote the reduced fluid pressure p_r and the average fluid density ρ_r normalized by the reference density ρ_0.

Secondly, re-arranging the transport equation $\phi(\partial\psi_i/\partial t) + \nabla\cdot[f_i\mathbf{v}_t] + \nabla\cdot[\lambda_i\mathbf{f}_i\nabla p_c] + \dot{\mathbf{q}}_i = 0$ we expand the capillary spreading into diffusion term and obtain

$$\phi\frac{\partial\psi_i}{\partial t} = -\mathbf{v}_t\cdot\frac{\mathrm{d}f_i}{\mathrm{d}\psi_i}\nabla\psi_i - \mathbf{f}_i\nabla\cdot\mathbf{v}_t - \nabla\cdot\left[\lambda_i\mathbf{f}_i\frac{\mathrm{d}p_c}{\mathrm{d}\psi_i}\nabla\psi_i\right] + \mathbf{q}_i\psi_i \tag{5}$$

In this formulation we try to moderate strong hyperbolicity of the initial transport equation by representing the divergence in the flow field of the phase i by source term $f_i\nabla\cdot[\mathbf{v}_t\,\mathrm{d}f_i/\mathrm{d}\psi_i]$ and treating capillary spreading of the saturation field by a diffusion term.

2.2. *Control volume hybrid finite element discretization*

We employ linear FEs to discretize the pressure equation (4) (similar to Reference [4]), using a dual CV/FE mesh to achieve conservation of fluid volume. In the CVFEM approach [6] FEs and CVs assume a complementary role in the spatio-temporal integration of fluid pressure, and Darcian fluxes are based on the fluid pressure derivative. A CV discretization that places cell boundary segments (referred to as facets) inside the FEs, where the FE interpolation functions are continuous, is required to integrate the discontinuous velocity arising from the differentiation of the piecewise linear pressure. Using node-centred CVs, the conservation law (5) can be solved. The difference from the traditional CV schemes in reservoir simulation (also multipoint flux method of Reference [2]) is in application of iso-parametric numerical integration on hybrid 3D CV/FE mesh together with a high-order TVD transport. For example, Figure 1(b) shows a 3D hybrid model with fractures meshed by tetrahedral/prism elements, and geometrically unconstrained regions meshed by hexahedra (mesh generated by the in-house Delaunay tetrahedral and indirect hybrid meshing code MezGen [7]). For the CVFEM models a hybrid mesh typically requires 25–30 per cent less memory than tetrahedral.

A subdivision of an FE into CV sectors is needed to determine fluxes across the facets. We do not actually store the CV mesh, but accumulate CV stencils directly in a solution matrix. Our approach applies to the models where CVs are composed of arbitrary combinations of

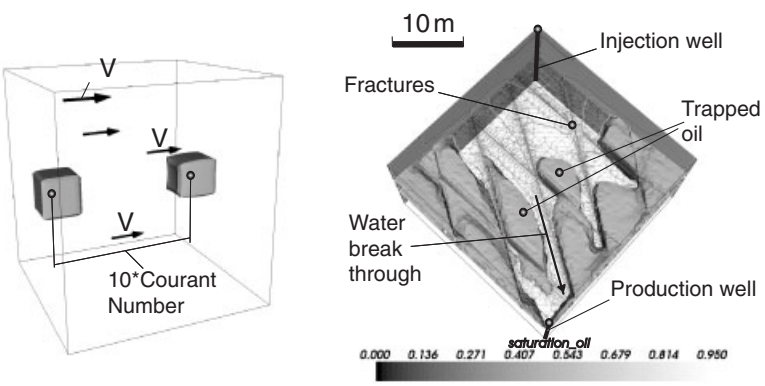

Figure 1. (a) Cube advection test; (b) contours of saturation in fractured reservoir.

3D FEs. The subdivision uses iso-parametric formulation, and we tabulate CV sectors in parametric space of different FE types. Each CV sector is a topological hexahedron and we perform the Gaussian volume and surface integration in the second parametric space, relating the mapped sector in the parametric space of an element to the unit cube [8]. Mesh deformation is possible and it does not compromise the accuracy of the numerical CV integration. In our formulation, all integration points and normals in CV sectors are pre-tabulated, improving the computational efficiency of integration during the run time.

It is important that the overall integral of a variable, discretized with node-centred piecewise constant CVs, is not exactly the same as the integral of a variable, discretized with piecewise linear FEs with the same nodes. Therefore, a transformation is required to map CV-discretized variables to FE nodes in order to interface the FE with the CV computations in a consistent manner. See Reference [9] for details.

2.3. Spatio-temporal integration: solution procedure

The pressure equation (4) is solved using a standard Bubnov–Galerkin FEM. Trilinear element interpolation functions N_i are used to integrate fluid pressure in space and are equivalent to the nodal weights W_i. The transient pressure is evolved using an implicit backward-Euler integration in time. The Darcian fluxes are based on the fluid pressure derivative (see Section 2.2) and we solve the transport equation (5) using the node-centred CVM with CV Darcian flux recovery. CV discretization of (5) gives a series of volume and surface integrals over the boundaries of each CV as well as volume integrals for distributed sources. CV integrals are expressed in terms of the piecewise constant CV interpolation functions M_i. For each FE, there are as many internal surfaces and integral contributions to CVs as there are connections between nodes. This set constitutes the CV stencil associated with the element, which is accumulated into a global solution matrix **A** and right-hand vector **b**. For example, the CV integrals for the first-order accurate upwind scheme, used as a first step in our high-order method, are

$$\phi \int_{\mathrm{CV}} M_i \frac{\partial \bar{\psi}_i}{\partial t} \,\mathrm{d}V + \int_{\mathrm{CV_{out}}} \mathbf{n} \cdot \mathbf{v}_\mathrm{t} \bar{\psi}_\mathrm{c} \,\mathrm{d}S + \int_{\mathrm{CV_{in}}} \mathbf{n} \cdot \mathbf{v}_\mathrm{t} \bar{\psi}_\mathrm{u} \,\mathrm{d}S - \int_{\mathrm{CV}} \mathbf{M}q \,\mathrm{d}V = 0 \tag{6}$$

Here *in* and *out* denote the in- and outgoing fluxes with regard to the CV cell i. The subscripts u, c refer to the far-field upstream and current CVs.

Initially we apply the first-order scheme with an implicit integration in time, performing an accumulation of integrated surface-normal fluxes into a solution matrix whose diagonal contains the pore volume of the ith CV, divided by an arbitrarily large time increment. Upwinding is achieved by discriminating incoming fluxes as off-diagonal couplings, while outgoing fluxes are decoupled through accumulation into the diagonal. A right-hand vector **b** contains the products of the pore volume and the current saturation divided by the time increment. The resulting sparse, positive definite, but asymmetric system of equations is solved using the algebraic multigrid method (AMG). The first-order scheme is overly diffusive and fails to preserve sharp saturation fronts as the transport equation (5) has a strongly hyperbolic character. This motivates the development of higher-order accurate method.

The higher-order accurate simulation of the mass-conservative transport of a scalar property (known as the Riemann problem) is a lively area of research and many robust schemes are available (e.g., References [10, 11]). To make a scheme second-order accurate, one typically

obtains an estimate of the gradient of the transported variable for each CV to find its values on the CV cell boundaries. To suppress oscillations, it is common to use slope limiters that guarantee the scheme becomes total variation diminishing (TVD, e.g. Reference [12]).

Temporal limiting, referred to as Θ-limiting, is introduced. Firstly, in the FE framework we interpolate $\hat{\psi}$ to the surface integration points k on the CV boundaries. Secondly, gradient estimates are assessed using the normalized variable approach, see Reference [9]. Thirdly, we apply a second-order Crank–Nicholson-type scheme to integrate a solution in time. However, for time steps greater than the mesh CN this approach can result in numerical oscillations. To avoid this, we introduce a parameter Θ, set to 0.5 for Crank–Nicholson and 1.0 for backward Euler schemes. The time differencing equation with the diffusive fluxes takes the form

$$\int_{\mathrm{CV}} \left(\frac{\bar{\psi}_i^{n+1} - \bar{\psi}_i^{n}}{\triangle t} - \bar{q} \right) dV = \int_{\mathrm{CV}} \Theta(\mathbf{n} \cdot \mathbf{v}_{\mathrm{t}} + K_n \mathbf{n} \cdot \nabla \hat{\psi}^{n+1}) \tilde{\psi}^{n+1} \, dS + \int_{\mathrm{CV}} (1 - \Theta)(\mathbf{n} \cdot \mathbf{v}_{\mathrm{t}} + K_n \mathbf{n} \cdot \nabla \hat{\psi}^{n}) \tilde{\psi}^{n} \, dS \tag{7}$$

For each time step and CV facet a value of Θ is calculated based on the satisfaction of the TVD criteria. Since backward Euler time differencing is TVD, the Θ-corrected Crank–Nicholson scheme is guaranteed to be TVD as Θ approaches 1. For the overall system of algebraic equations, this applies with the proviso that the diagonal of the solution matrix remains positive. This extra constraint can be taken into account when Θ is calculated. We achieve this by measuring the temporal change in both upstream and downstream facet fluxes, increasing Θ gradually from 0.5 to 1.0 as the local CFL limit is approached.

Finally, we apply the following flux-limited high-order CV discretization of the transport equation in the integral form:

$$\phi \int_{\mathrm{CV}} M_i \frac{\partial \bar{\psi}_i}{\partial t} \, dV + \int_{\mathrm{CV}} \mathbf{n} \cdot \mathbf{v}_{\mathrm{t}} \tilde{\psi}_k \, dS - \int_{\mathrm{CV}} M_i q \, dV = 0 \tag{8}$$

where the flux-limited high-order FE approximation $\tilde{\psi}_k$, replaces the upwind first-order approximation $\bar{\psi}_{\mathrm{u}}$ in (8) and the source q also includes flow-field-related divergence terms. Due to the flux-limiting, Equation (8) is now non-linear, and needs to be transformed into a linear system of equations. We achieve this by means of a Picard iteration.

3. RESULTS

The scheme has been implemented as an extension of the CVFEM code Radiant, developed by Pain *et al.* [9]. Time stepping efficiency is demonstrated by the advection test. Figure 1(a) presents a constant velocity (shown as arrows) transport of the cubical profile on a hybrid mesh, generated by the MezGen mesher [7]. Here we use time steps 10 times greater than the mesh CN. The dispersion of the cubical profile is minimal as the scheme remains stable and second-order accurate in space and time.

Figure 1(b) shows a $30 \times 30 \times 10$ metre hybrid model of the fractured reservoir with 167 171 nodes and 713 071 elements, generated by the MezGen. Multiphase flow is considered. Water

is injected at the injection well, oil is extracted at the production well. The injection pressure is 1×10^{14} Pa. The matrix permeability is $1 \times 10^{-15}\,\mathrm{m}^{-2}$, the porosity is 0.3, fractures have a permeability of $1 \times 10^{-12}\,\mathrm{m}^{-2}$ and the porosity 0.9. We use Brooks–Corey [5] relative permeability model for the matrix. Oil and water viscosity are equal. Iso-contours of oil saturation 0.5 (initial oil saturation is 0.95) are shown after 35.7 days of water injection. A high-order scheme is required to capture saturation fronts accurately on 3D fracture-matrix interfaces. The small size of mesh elements dictates the usage of new implicit time stepping. Figure 1(b) shows the water break through fractures and large amounts of oil trapped in the matrix. The test in Figure 1(b) confirms efficiency of the proposed method in a realistic reservoir simulation.

4. CONCLUSIONS

This paper contributes implicit pressure–implicit saturation high-order CVFEM method for multiphase fluid flow simulations on hybrid meshes with discrete volumetric fractures. Generalization of a known CVFEM transport algorithm to hybrid meshes is provided. Simultaneously, the method overcomes the CFL constraint on transport simulations with implicit variable order time stepping. The method is successfully applied to the two-phase transport equation (5) with gravitational and capillary terms on complex hybrid 3D meshes.

Preliminary results suggest that the scheme is very well suited for the simulation of a fluid flow in a fractured porous media, because: (1) the CFL condition no longer limits time-step size; (2) the mass conservation equation is solved directly using the CVM; (3) propagating saturation can be modelled with second-order accuracy in space and in time.

ACKNOWLEDGEMENTS

Authors would like to thank the sponsors of the ITF project ‘Improved Simulation of Fractured Reservoirs’ for their financial support and Dr K. Stuben for providing the AMG solver.

REFERENCES

1. Skjaeveland SM, Kleppe J (eds). Recent advances in improved oil recovery methods for North Sea sandstone reservoirs. *SPOR Monograph*. Norwegian Petroleum Directorate: Stavanger, 1992; 335. ISBN 82-7257-340-7.
2. Aavatsmark I, Barkve T, Boe O, Mannseth T. Discretization on unstructured grids for inhomogeneous, anisotropic media. Part I: derivation of the methods. *SIAM Journal on Scientific Computing* 1998; **19**(5): 1700–1716.
3. Naji HS, Kozemi H. A fully implicit, three-dimensional, two-phase, control volume finite element model for the simulation of naturally fractured reservoirs. *SPE 36279*, 1996.
4. Huber R, Helmig R. Multi-phase flow in heterogeneous porous media: a classical finite element method versus an implicit pressure–explicit saturation-based mixed finite element control volume approach. *International Journal for Numerical Methods in Fluids* 1999; **29**:899–920.
5. Brooks RH, Corey AT. Hydraulic properties of porous media. *Hydrol. Pap*., vol. 3. Colorado State University, 1964.
6. Baliga BR, Patankar SV. A new finite-element formulation for convection–diffusion problems. *Numerical Heat Transfer* 1980; **3**:393–409.
7. MezGen: an unstructured Delaunay/hybrid mesh generator with direct CAD interface. http://www.geocities.com/aamezentsev/Mezgen.html (17 October 2004).
8. Mezentsev AA, Matthai SK, Pain CC, Eaton MD. A bounded control volume hybrid finite element method for subsurface flow simulations. In *European Congress on Computational Methods in Applied Sciences and*

Engineering 24–28 July 2004, Neittaanmaki P, Rossi T, Majava K, Pironneau O (eds), Jyväkylä, Finland, vol. 1, 2004; 221–241. ISBN 951-39-1869-6.
9. Pain CC, Gomes JLMA, Eaton MD, Goddard AJH. Numerical transport methods for radiation and multi-phase fluid flow modeling. *Nuclear Science and Engineering* 2001; **138**:78–95.
10. Harten A, Osher S. Uniformly high-order accurate nonoscillatory schemes, I. *SIAM Journal on Numerical Analysis* 1987; **24**:279–309.
11. Liu XD, Lax PD. Positive schemes for solving multi-dimensional hyperbolic systems of conservation laws. *Computational Fluid Dynamics Journal* 1996; **5**:133–156.
12. LeVeque RJ. *Finite Volume Methods for Hyperbolic Problems*. Cambridge University Press: Cambridge, 2003.

